2024 IEEE International Conference on Robotics and Automation (ICRA 2024)
May 13-17, 2024. Yokohama, Japan

Towards Solving Cable-Driven Parallel Robot Inaccuracy due to Cable Elasticity

Adolfo Suárez Roos[1], Zane Zakşe[1], Tahir Rasheed[1], Nicolò Pedemonte[1], and Stéphane Caro[2]

***Abstract*— Cable elasticity can significantly impact the accuracy of Cable-Driven Parallel Robots (CDPRs). However, it's frequently disregarded as negligible in CDPR simulations and designs. In this paper, we propose a numerical approach, referred to as SEECR, which is designed to estimate the behavior of a CDPR featuring elastic cables while ensuring the Static Equilibrium (SE) of the Moving-Platform (MP). By modeling the cables as elastic springs, the proposed approach correctly predicts which cables become slack, estimates the tension distribution among cables and computes unwanted MP motions, allowing to predict the impact of design choices. The results have been validated experimentally on two cable types and configurations.**

I. Introduction

Cable-Driven Parallel Robots (CDPRs) represent a specific category of parallel robots in which the Moving-Platform (MP) is connected to a fixed base frame by cables. The translation and rotation motions of the MP are achieved through the synchronized control of the cable lengths. CDPRs can be used in many applications such as large payload handling over a large workspace (WS) [1], [2], fast pick-and-place tasks [3] and rehabilitation [4]. As the research interest in large CDPRs grows [5]–[9], several cable characteristics, such as sag and elasticity can no longer be neglected.

If cable elasticity is not modelled, the actual MP pose is going to be different from the expected one. This is because the cables are longer than predicted due to elasticity. Moreover, with increased CDPR size, cable length difference also increases and leads to substantial MP pose errors. Indeed, if the model is not close enough to the real CDPR, its accuracy is going to be significantly affected.

When cable elasticity is modelled, it is assumed to be a linear spring [10]–[14], while some studies have shown that a non-linear model should be used [15]. Furthermore, a certain hysteresis can sometimes be observed [16], [17]. Having identified the elasticity of cables, one can then estimate the stiffness of a CDPR [10], [13]–[15] and use control approaches that are stiffness-oriented [11]. Note that recently neural networks have been used to solve the inverse kinematic model with elastic cables [18], [19].

*Supported by IRT Jules Verne (French Institute of Research and Technology in Advanced Manufacturing Technologies for Composite, Metallic and Hybrid Structures)

[1]Nantes Université, IRT Jules Verne, F-44000 Nantes, France, adolfo.suarez-roos@irt-jules-verne.fr, tahir.rasheed@irt-jules-verne.fr, zane.zake@irt-jules-verne.fr, nicolo.pedemonte@irt-jules-verne.fr

[2]Nantes Université, École Centrale Nantes, CNRS, LS2N, UMR 6004, F-44000 Nantes, France stephane.caro@ls2n.fr

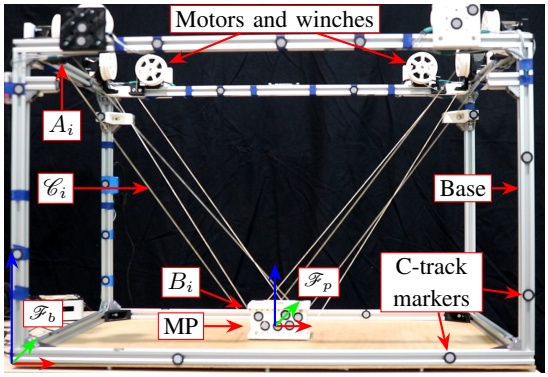

Fig. 1. CDPR prototype named DemoBot

Sometimes it is assumed that the cable is not only elastic but is also sagging due to its own mass. The sagging cable is usually modelled as a catenary [20]–[23], creating a complex model. However, it was shown in [24] that the model can be linearized without significant loss of accuracy.

Depending on the targeted level of accuracy, the modelling of cable elasticity can be necessary. Thus, one needs to be able to rapidly evaluate the CDPR behavior given its model and cable elasticity coefficient. In this paper, a Solver for Equilibrium of Elastic Cable Robots (SEECR) is proposed. It takes cable elasticity into account while finding the MP pose for which the Static Equilibrium (SE) is held. It allows us to know the actual MP pose, including unwanted tilt, also named parasitic tilt, that can be generated from a non-optimal cable configuration. Hence, SEECR can be used as a tool to evaluate the effect of cable configurations and overall CDPR model on the MP behavior. Moreover, SEECR can determine the actual MP pose even when the desired pose lies outside the robot's Static-Feasible Workspace (SFW). Therefore, knowing the CDPR behavior beyond their SFW allows us to potentially utilize more of the CDPR footprint.

In this paper three CDPR models are considered: (i) an under-actuated two-cable CDPR to explain in detail SEECR function; (ii) a suspended four-cable three-Degree of Freedom (DoF) planar CDPR with two cable configurations; (iii) a suspended 8-cable 6-DoF spatial CDPR with two cable configurations. The latter corresponds to a real CDPR prototype, shown in Fig. 1, and all the experiments are repeated on it to practically validate the solver.

II. Classic Kinematic Model of a CDPR

In this paper, a small CDPR named DemoBot, shown in Fig. 1, is presented. Its MP is pulled by $m = 8$

TABLE I

NOTATION USED THROUGHOUT THE PAPER

- $\mathscr{C}_i$ - ith cable; $i = 1, \ldots, m$ and $m = 8$
- $\mathscr{F}_b(x, y, z)$ and $\mathscr{F}_p(x_p, y_p, z_p)$ are the base and MP frames resp.
- P - tracking point of the MP
- A_i - cable exit points associated with $\mathscr{C}_i$
- B_i - cable anchor points associated with $\mathscr{C}_i$
- ${}^b\mathbf{a}_i$ - Cartesian coordinates of A_i expressed in $\mathscr{F}_b$
- ${}^p\mathbf{b}_i$ - Cartesian coordinates of B_i expressed in $\mathscr{F}_p$
- $\mathbf{l}_i = {}^b\mathbf{a}_i - {}^b\mathbf{b}_i$ - cable vector pointing from B_i to A_i
- l_i - cable length of $\mathscr{C}_i$
- ${}^b\mathbf{u}_i = \frac{\mathbf{l}_i}{||\mathbf{l}_i||_2}$ - unit vector of $\mathscr{C}_i$ pointing from B_i to A_i
- $\mathbf{w}_e$ - external wrench acting on the MP
- τ_i - tension in cable $\mathscr{C}_i$. Since cables can only push but not pull, the tensions should remain non-negative, *i.e,* $\tau_i \geq 0$, in order for the $\mathscr{C}_i$ to be able to apply a wrench onto the MP
- ${}^b\mathbf{p} = [p_x, p_y, p_z, \alpha, \beta, \gamma]$ - MP pose expressed in $\mathscr{F}_b$
- $\delta\mathbf{p} = [\delta p_x, \delta p_y, \delta p_z, \delta\alpha, \delta\beta, \delta\gamma]$ - Deviation in the MP pose expressed in $\mathscr{F}_b$
- ${}^b\mathbf{R}_p$ and ${}^b\mathbf{t}_p$ - rotation matrix and translation vector of the MP expressed in $\mathscr{F}_b$

cables. Its size is $80\,\text{cm} \times 50\,\text{cm} \times 50\,\text{cm}$. The MP size is $10.2\,\text{cm} \times 4.4\,\text{cm} \times 3.6\,\text{cm}$ and its mass is $0.4\,\text{kg}$. The notation used in this paper is shown in Table I.

The anchor point B_i for $\mathscr{C}_i$ is expressed in $\mathscr{F}_b$ as:

$$ {}^b\mathbf{b}_{i0} = {}^b\mathbf{R}_{p_0}\,{}^p\mathbf{b}_i + {}^b\mathbf{t}_{p_0} \tag{1} $$

${}^b\mathbf{b}_{i0}$ denotes the initial Cartesian coordinates vector of the anchor points considering cables as non-elastic. The corresponding initial cable length denoted as l_{i0}, is expressed as:

$$ l_{i0} = ||{}^b\mathbf{a}_i - {}^b\mathbf{b}_{i0}||_2 \tag{2} $$

The MP is in SE if the external wrenches, including the gravity wrench, acting onto the MP, can be counterbalanced by the sum of non-negative cable tensions, expressed as [10]:

$$ \mathbf{W}\boldsymbol{\tau} + \mathbf{w}_e = 0 \tag{3} $$

where $\mathbf{w}_e$ is external wrench applied to the MP, $\boldsymbol{\tau} = [\tau_1, \tau_2, \ldots, \tau_m]$ is the cable tension vector, and $\mathbf{W}$ is the wrench matrix of DemoBot that is defined as:

$$ \mathbf{W} = \begin{bmatrix} {}^b\mathbf{u}_1 & \ldots & {}^b\mathbf{u}_m \\ {}^b\mathbf{R}_p\,{}^p\mathbf{b}_1 \times {}^b\mathbf{u}_1 & \ldots & {}^b\mathbf{R}_p\,{}^p\mathbf{b}_m \times {}^b\mathbf{u}_m \end{bmatrix} \tag{4} $$

III. Analytical vs Numerical Solution

A. Analytical Solution

To illustrate the analytical approach, a case study of an under-actuated planar CDPR [25], [26] with two cables is presented here. Its MP pose ${}^b\mathbf{p}$ is defined as (p_x, p_y, θ). Using (1), (2) and (3) for a planar under-actuated CDPR presented in Fig. 2, the angle θ of the MP is symbolically solved and expressed as:

$$ \theta = 2\text{atan}\left(\frac{2p_x^2 - 2p_x(a_{1x} - a_{2x}) + 2a_{1x}a_{2x} + S_q}{p_x p_y(a_{1y} + a_{2y} - 2) + p_y(a_{1x} + a_{2x}) - a_{1x}a_{2y} - a_{2x}a_{1y}}\right) \tag{5} $$

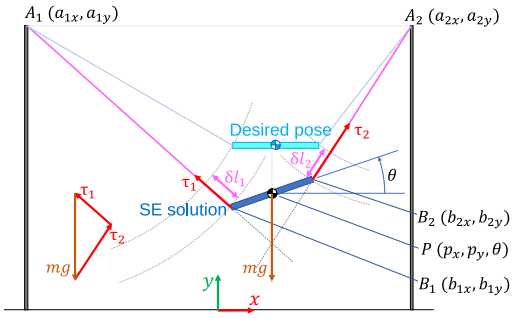

Fig. 2. A planar under-actuated CDPR parameterization

where

$$ \begin{aligned} S_q = \sqrt{} & 4p_x^4 - 8p_x^3a_{1x} - 8p_x^3a_{2x} + 4p_x^2a_{1x}^2 + 16p_x^2a_{1x}a_{2x} + \\ & 4p_x^2a_{2x}^2 + 4p_x^2p_y^2 - 4p_x^2p_ya_{1y} + 6p_xa_{1x}p_ya_{2y} - \\ & 4p_x^2p_ya_{2y} + p_x^2a_{1y}^2 + 2p_x^2a_{1y}a_{2y} + p_x^2a_{2y}^2 - \\ & 8p_xa_{1x}^2a_{2x} - 8p_xa_{1x}a_{2x}^2 - 4p_xa_{1x}p_x^2 - 2p_xa_{1x}a_{2y}^2 - \\ & 2p_xa_{1x}a_{1y}a_{2y} + 2p_xa_{1x}p_ya_{1y} - 2p_xa_{2x}a_{1y}a_{2y} - \\ & 4p_xa_{2x}p_y^2 + 6p_xa_{2x}p_ya_{1y} + a_{1x}^2p_y^2 + 2p_xa_{2x}p_ya_{2y} - \\ & 2p_xa_{2x}a_{1y}^2 + 4a_{1x}^2a_{2x}^2 + a_{1x}^2a_{2y}^2 + 2a_{1x}a_{2x}p_x^2 - \\ & 2a_{1x}^2p_ya_{2y} + a_{2x}^2p_y^2 - 2a_{2x}^2p_ya_{1y} + a_{2x}^2a_{1y}^2 - \\ & 2a_{1x}a_{2x}p_ya_{1y} - 2a_{1x}a_{2x}p_ya_{2y} + 2a_{1x}a_{2x}a_{1y}a_{2y} \end{aligned} \tag{6} $$

As the system is under-actuated, the MP angle is not controlled and it always tilts toward the center. The middle of the bar-shaped MP shown in Fig. 2 coincides with the center of mass (CoM).

The unique value for θ found by this analytical solution for each platform position (p_x, p_y) constitutes the manifold shown in Fig. 3. The manifold represents all the SE poses of this two-cable robot. Note that the lower edge of the manifold is almost a straight line, meaning that the tilt evolution is almost linear when the robot is close to the ground. On the contrary the S shape of the upper edge indicates that the MP remains quite horizontal when x is closer to the center and then rapidly tilts when approaching large x values. This is also visible in Fig. 4 where the following poses are represented: (i) in cyan, the desired poses, with $\theta = 0°$ (note that these poses can be outside the manifold); (ii) the green analytical solutions, showing the tilt angle the MP must have to be in SE at the desired position; (iii) the blue solutions, computed by SEECR using the cyan as a starting point and drifting away from it until equilibrium is found. As expected, the two solutions are different but both lie on the manifold.

The analytical form of the solution is complex and the complexity will increase substantially when dealing with higher DoFs CDPR with more cables. Moreover, the incorporation of cable stiffness will introduce further complexity to the system in order to achieve an analytical solution.

B. Numerical solution : SEECR

As shown in [22] determining inverse kinematics solutions considering cable deformation in analytic form can

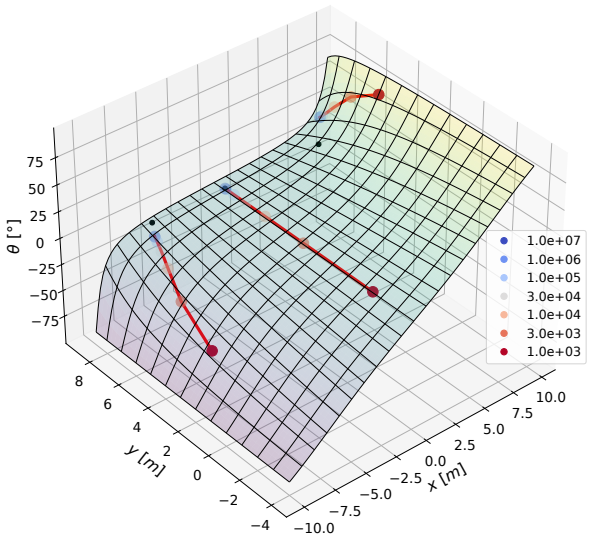

Fig. 3. Solution manifold for $m = 2$, where: black dots are the desired MP poses and are outside the manifold; the curves show the evolution of the associated solutions depending on the cable elasticity

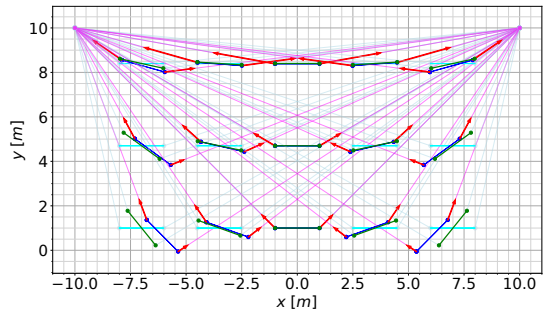

Fig. 4. Plot of MP poses for $m = 2$, where: the desired MP pose is in cyan (not in manifold); the analytically found SE orientation at the desired pose is in green (in manifold); and the actual MP pose found by SEECR given the desired pose as an input is shown in blue (in manifold)

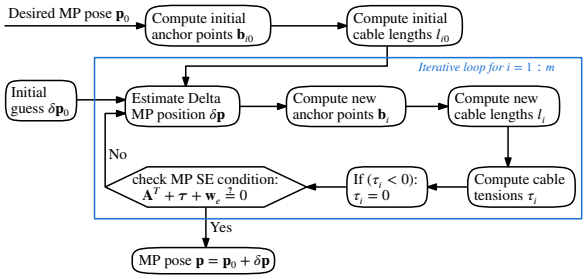

Fig. 5. SEECR Algorithm

be quite challenging. Thus, usually a numerical approach to determine all possible inverse kinematics solutions for any number of cables is chosen. In this paper, we propose a numerical approach referred to as Solver for Equilibrium of Elastic Cable Robots (SEECR) that finds the SE pose of the MP based on a desired pose. The key idea is that the cables do not provide any tension at their initial (nominal) lengths. Deviations around the desired pose will result in changes of the anchor point coordinates which results in the cables becoming longer or shorter. Longer cables will apply tensions proportional to their elongation while shorter cables are slack. The SEECR will iteratively search for a pose that minimizes the error of the SE equation. Different solvers from the python scipy.optimize library [27] were tested. In particular (i) fsolve, which produced the best equilibrium values; and (ii) least squares, which provided more robust results in many situations. These solvers will search for the pose that corresponds to the roots or the local minimum for the SE. Both take as input a non-linear set of equations and an initial estimation. In addition, both compute numerically a local Jacobian $\boldsymbol{\partial F / \partial p}$ to guide the estimation process. The algorithm of the SEECR is shown in Fig. 5. SEECR iteratively looks for MP poses that satisfy the SE given by (4), and exits after converging to a solution or detecting that progress is no longer observed.

1) Initial pose: The first step is to input the desired pose. This corresponds to the equilibrium solution if there is no gravity or external forces acting on the MP. If the desired pose is feasible, it is also the solution for non elastic cables.

2) Initial Anchor points: From the given initial pose, initial values of all anchor points ${}^b\mathbf{b}_{i0}$ are computed using (1).

3) Initial cable lengths: Knowing the anchor points, the initial lengths of all cables l_{i0} are computed using (2).

4) Initial guess: A naive guess $\delta\mathbf{p}_0$ of the solution is applied by assuming that the MP will fall vertically due to its weight as $\delta\mathbf{p}_0 = (m_g g l_{vmean})/k_c$, where m_g is the MP mass and g is the gravity. l_{vmean} is the mean value of the vertical component l_{zi} of all cables: $l_{vmean} = \sum_{i=1}^{m} l_{zi}$. $k_c = ES$ represents the cable stiffness, where E is the Young's modulus and S is the cross-sectional area of the cable.

The solver's iterative process commences at this point, initiating with the initial guess.

5) Calculation of new cable anchor points: The novel MP pose and the associated anchor points are computed as:

$$ {}^b\mathbf{p} = {}^b\mathbf{p}_0 + \delta\mathbf{p} \tag{7} $$

$$ {}^b\mathbf{b}_i = {}^b\mathbf{R}_p {}^p\mathbf{b}_i + {}^b\mathbf{t}_p \tag{8} $$

where ${}^b\mathbf{t}_p$ and ${}^b\mathbf{R}_p$ are the new translation vector and rotation matrix of the MP.

6) Calculation of new cable lengths: The corresponding new cable lengths are computed using the updated cable anchor points:

$$ l_i = ||{}^b\mathbf{a}_i - {}^b\mathbf{b}_i||_2 \tag{9} $$

7) Calculation of elastic cable tensions: Considering a cable as a spring means that in its rest length the cable has no tension. As a consequence a cable can only apply a force if it is elongated. Furthermore each cable tension τ_i is proportional to its elongation δl_i and inversely proportional to its initial length l_{i0} [10], [15]:

$$ \tau_i = k_{ci} \frac{\delta l_i}{l_{i0}} \tag{10} $$

where $\delta l_i = l_i - l_{i0}$ is the difference between the estimated and initial cable lengths, resp.

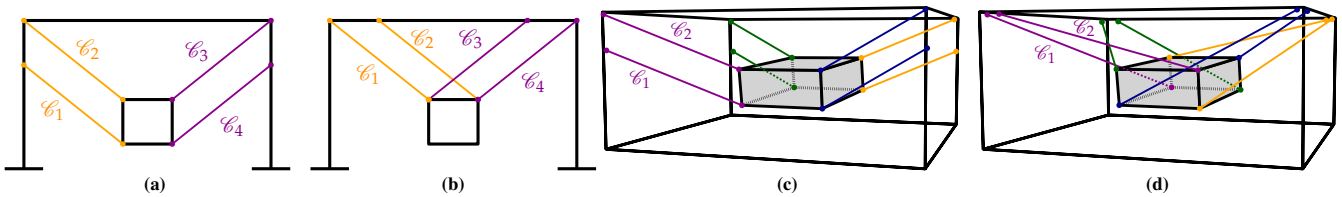

Fig. 6. Case studies: **(a)** four-cable vertical planar CDPR; **(b)** four-cable horizontal planar CDPR; **(c)** Eight-cable vertical spatial CDPR; **(d)** Eight-cable crossed spatial CDPR (Cogiro configuration)

8) Enforcing Non-Negative cable tensions: Since cables cannot apply compression, the desired solution should only include non-negative cable tensions. Hence, any negative cable tension is set to zero:

$$\tau_i = \begin{cases} \tau_i, & \text{for } \tau_i \geq 0, \\ 0, & \text{for } \tau_i < 0, \end{cases} \tag{11}$$

9) Static Equilibrium: Once the tensions and cable directions are known, the SE can be computed using (3). If the SE condition is satisfied, the iterative loop concludes and the final MP pose is returned by the solver as (7). Otherwise, if the SE condition is not met, the iteration continues with a new estimation in the following step.

10) Solver updates the deviation in the MP pose: At each iteration, a novel MP pose deviation $\delta\mathbf{p}$ is computed by the solver (fsolve or least squares).

The SEECR has been examined on multiple case studies depicted in Fig. 6 and presented hereafter.

C. Case study: Planar under-actuated CDPR with $m = 2$ cables

This case is shown in Figs. 2, 3 and 4. In Fig. 3 the desired poses with $\theta = 0°$ are shown as black dots. Note that only one is on the solution manifold, while the other two cannot be reached by this CDPR. The corresponding SE pose is found using SEECR and it is a function of the cable elasticity. Indeed, as shown with blue-to-red curves in Fig. 3, the more elastic the cable the smaller the y-coordinate of the MP and thus the further the actual pose from the desired pose.

In Fig. 4 the desired poses are shown in cyan. Once again as the desired orientation is $\theta = 0°$, most of these poses are not on the manifold. The blue poses are the corresponding actual MP poses found by SEECR for each of the desired poses. Note that the blue poses do not coincide with the analytically found green poses, because cable elasticity leads to parasitic tilt, but also to a lateral motion towards the center of the workspace and a downward motion.

D. Case study: Planar CDPR with $m = 4$ cables

Two planar CDPRs with distinct cable configurations, have been investigated. The first case study involves a four-cable CDPR with a vertical parallelogram-like configuration [28], [29] shown in Fig. 6a and 7. The second configuration features a horizontal parallelogram-like cable arrangement, depicted in Fig. 6b and Fig. 8.

Having parallel cables seems like the perfect approach to avoid the platform unexpected tilts. However, while the horizontal arrangement achieves this, the vertical one completely fails. In fact, the left and right parallelograms will only retain their shape if the cable lengths are equal which implies that both cable elongations and therefore both cable tensions need to be equal. As shown in Fig. 9, for the horizontal arrangement, point H is the intersection of the midlines of the parallel cables. By computing the equilibrium around point H, it is observed that, if both the cables from the left side are having the same cables tensions, they will generate no torque on the MP. Same behavior can be observed from the cables on the opposite side. The gravity wrench passes through point H only at zero rotation. As a result, the platform will only remain in rotational equilibrium at zero orientation. Given that, it is possible to find tension values that add up to cancel the vertical gravity while their

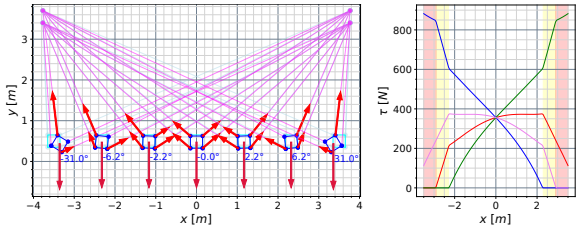

Fig. 7. Vertical parallelogram-like configuration: (left) different platform poses at SE; (right) cable tensions, where the zone with one slack cable is shown in yellow and with two slack cables in red

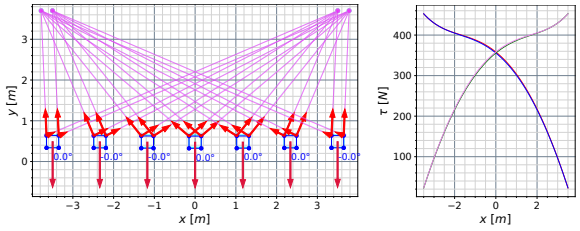

Fig. 8. Horizontal parallelogram-like configuration: (left) different platform poses at SE; (right) cable tensions

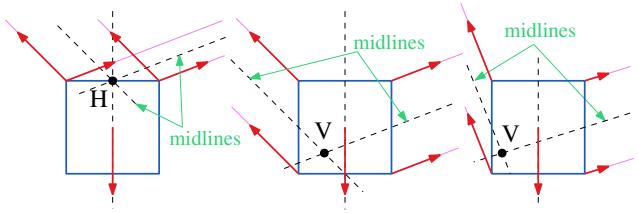

Fig. 9. Tilt conditions for four-cable planar CDPR: (left) horizontal; (middle) and (right) vertical arrangement in two different MP poses

horizontal components cancel each-other. Thus, the SE is reached without tilting. Fig. 8 shows no tilt and equal tensions in the cables on each side.

For the vertical arrangement in Fig. 9, point V is the intersection of the midlines of the parallel cable and the only point where the equal tensions on both sides would produce zero torque. Note that the coordinates of this point depend on the MP pose and can even be outside the MP. The gravity force only passes through this point when the platform is in the center. For any other position a tilt is required in order to achieve equilibrium. An additional interesting point can be illustrated in Fig. 7. As the robot approaches to the boundaries, the tension in some cables progressively disappear and the CDPR transitions from four tensed cables to three and then to two. Beyond this point, the four-cable CDPR behave exactly like a two-cable under-actuated CDPR. Its solution can be found analytically and a manifold can be computed. The manifold is different the left and right sides since the cables under tension are not the same.

E. Case study: Spatial CDPRs with $m = 8$ cables

As a spatial CDPR case study, the DemoBot shown in Fig. 1 was studied by employing two distinct cable configurations. The first configuration, referred to as the Cogiro configuration [6] is illustrated in Fig. 6d. The second configuration adopts a vertical parallelogram-like setup [10], [30], as shown in the Fig. 6c.

The results from SEECR can be seen in Fig. 10 and 11. The green WS shown in the two figures is the SFW that was computed using ARACHNIS [31], [32]. The behavior of the CDPR is similar as in the previous case study.

Using the Cogiro configuration of the DemoBot, which is a well-established cable layout for withstanding external wrenches, the CDPR maintains a steady rotation of the MP. On the other hand, in case of parallel configuration, it can be seen that as the robot moves away from the center of the structure, the MP experiences significant tilting, and tension in some cables rapidly goes to zero. Indeed, as the MP leaves the SFW, the tilt becomes unavoidable. However, as SEECR allows us to predict such a behavior, the CDPR could be used outside the SFW in a degraded state.

F. Performance of SEECR

The SEECR performance was assessed on an Intel i7-10850H CPU clocked at 2.7GHz, using Python 3.11.5 on Windows 10 OS. In the best and worst-case scenarios, solutions were found after 14 and 286 iterations or 2 ms and 61 ms, resp., with each iteration taking 0.21 ms. Less iterations were needed at the center of the WS, where initial guess and the actual MP pose are close.

IV. Experimental Results

To validate the SEECR, several experiments were conducted using DemoBot and the ground truth was measured by Creaform C-track that can achieve 0.065 mm volumetric accuracy[1]. The experiments were carried out by employing

[1]https://www.creaform3d.com/en

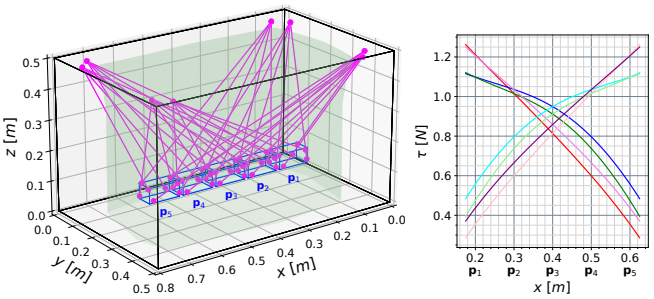

Fig. 10. DemoBot with Cogiro configuration: (left) different platform poses at SE and the SFW shown in green; (right) cable tensions

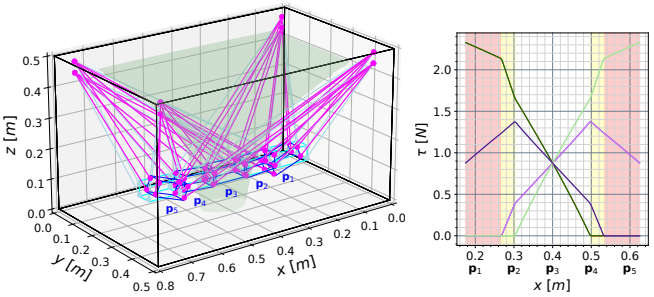

Fig. 11. DemoBot with vertical parallel configuration: (left) different platform poses at SE and the SFW shown in green; (right) cable tensions, where the zone with two slack cables is shown in yellow and with four slack cables in red

TABLE II

Cable exit and anchor point coordinates

Cogiro configuration A_i in $\mathscr{F}_b$ and B_i in $\mathscr{F}_p$, m			
A_1	$[0.08; 0.04; 0.485]^\top$	B_1	$[0.04; -0.03; 0.018]^\top$
A_2	$[0.04; 0.08; 0.485]^\top$	B_2	$[-0.0515; 0.022; -0.018]^\top$
A_3	$[0.04; 0.42; 0.485]^\top$	B_3	$[-0.0515; -0.022; 0.018]^\top$
A_4	$[0.08; 0.04; 0.485]^\top$	B_4	$[0.04; 0.03; -0.018]^\top$
A_5	$[0.72; 0.46; 0.485]^\top$	B_5	$[-0.04; 0.03; 0.018]^\top$
A_6	$[0.76; 0.42; 0.485]^\top$	B_6	$[0.0515; -0.022; -0.018]^\top$
A_7	$[0.76; 0.08; 0.485]^\top$	B_7	$[0.0515; 0.022; 0.018]^\top$
A_8	$[0.72; 0.04; 0.485]^\top$	B_8	$[-0.04; -0.03; -0.018]^\top$
Parallel configuration A_i in $\mathscr{F}_b$ and B_i in $\mathscr{F}_p$, m			
A_1	$[0.04; 0.04; 0.486]^\top$	B_1	$[-0.0515; -0.022; 0.018]^\top$
A_2	$[0.04; 0.04; 0.450]^\top$	B_2	$[-0.0515; -0.022; -0.018]^\top$
A_3	$[0.04; 0.46; 0.486]^\top$	B_3	$[-0.0515; 0.022; 0.018]^\top$
A_4	$[0.04; 0.46; 0.450]^\top$	B_4	$[-0.0515; 0.022; -0.018]^\top$
A_5	$[0.76; 0.46; 0.486]^\top$	B_5	$[0.0515; 0.022; 0.018]^\top$
A_6	$[0.76; 0.46; 0.450]^\top$	B_6	$[0.0515; 0.022; -0.018]^\top$
A_7	$[0.76; 0.04; 0.486]^\top$	B_7	$[0.0515; -0.022; 0.018]^\top$
A_8	$[0.76; 0.04; 0.450]^\top$	B_8	$[0.0515; -0.022; -0.018]^\top$

the same distinct configurations discussed in Section III-E. The corresponding cable exit and anchor point coordinates are shown in Table II. Furthermore, to ensure a thorough evaluation, we tested two distinct types of cables: (i) Vectran cable with 0.7 mm diameter; (ii) fishing cable with 0.4 mm diameter. This allowed us to assess the SEECR performance under various conditions, taking into account different cable configurations and materials.

A simple linear trajectory along x from $x = 0.17$ m to

$x = 0.63\,\text{m}$ was repeated for all configurations at two distinct heights of $z_1 = 0.1\,\text{m}$ and $z_2 = 0.2\,\text{m}$. The desired trajectory required a constant MP orientation throughout. The experimental results are shown in Figs. 12a and 12b. The former presents the deviation from the desired MP pose along z while the latter illustrates the platform rotation about y. It is evident that there are two very different trends: the curves representing the Cogiro configuration exhibit an impressive degree of linearity, closely approximating an ideal straight trajectory. In contrast, the curves associated with the parallel configuration display a notable and persistent deviation. Indeed, regardless of the chosen cable material, the parallel configuration leads to a significant tilt of approximately 20° at both ends of the trajectory. This tilt is accompanied by a large deviation along z of about 15 mm. Notably, at the extreme points of the recorded trajectories, the MP never reaches the desired position along x. These observations highlight the substantial disparity in DemoBot's behavior depending on chosen cable configuration. Regarding the cable material, since fishing cable is more elastic (the stiffness coefficient is approximately 10 times smaller), an additional deviation is anticipated along z for the experiments conducted with the aforementioned cables. The phenomena can be observed in Fig. 12a where the cyan curve is consistently lower than the brown curve.

The trajectories obtained by SEECR are close to the measured ones. SEECR correctly estimated the behavior of the robot, yet subtle disparities are evident. For example, in Fig. 12b, the blue estimation closely aligns with the cyan measurement, with the exception of a slight deviation at the initial segment of the trajectory. Similarly, when comparing the brown and red curves, a minor discrepancy is noticeable at the far-right portion. These variances can be attributed to the initialization procedure of DemoBot. Prior to each experiment, the MP was manually positioned in the initial pose, resulting in minor inaccuracies that persist throughout the trajectory.

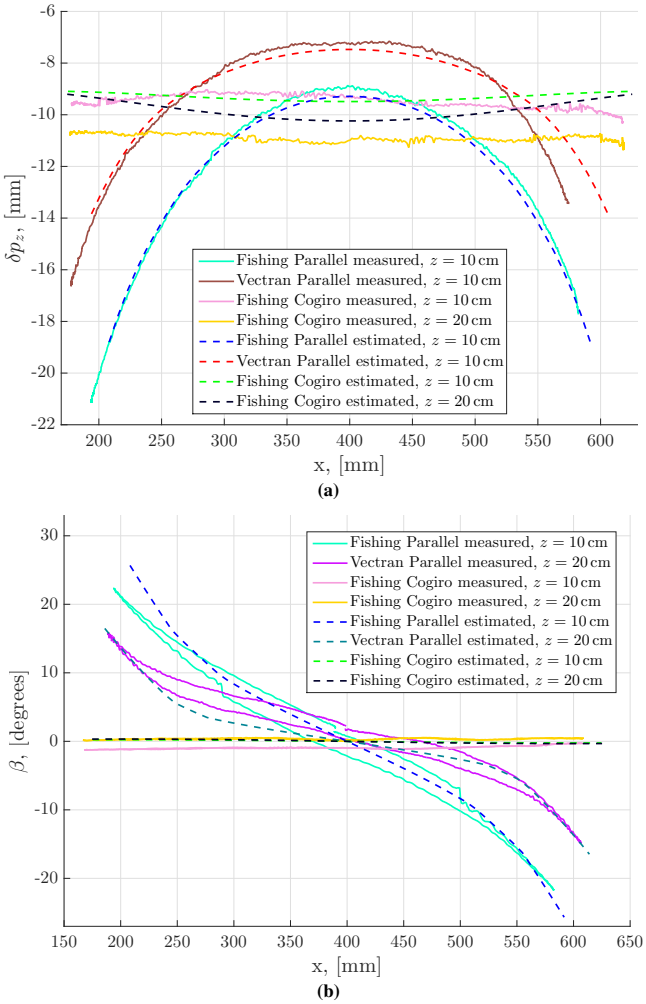

Fig. 12. Experimental results: **(a)** deviation from the desired height along z-axis; **(b)** Mp rotation about y-axis

V. Discussions and Future Work

In this paper we proposed a numerical approach, referred to as SEECR, to estimate the behavior of a Cable-Driven Parallel Robot (CDPR) featuring elastic cables while ensuring the Static Equilibrium (SE) of the Moving-Platform (MP). SEECR was shown to correctly predict the cables becoming slack, to estimate the tension distribution among cables and correctly simulate unwanted MP motions. There are numerous potential applications for SEECR. One of its most practical uses lies in its capability to swiftly assess any CDPR model in terms of parasitic motion, such as undesired tilt of the MP due to the chosen cable configuration and thus the reduced workspace. To illustrate the effectiveness of SEECR, two case studies were considered: one involving a four-cable planar CDPR and another using an eight-cable spatial CDPR, each with two distinct cable configurations. The results clearly demonstrated that not all cable configurations are uniformly effective, underscoring the importance of selecting preferred configurations over others. However, if a sub-optimal configuration must be chosen, SEECR allows us to know the CDPR behavior outside the Static Feasible Workspace (SFW) and thus continue using the robot even in a degraded state.

The spatial CDPR cable configurations were subsequently evaluated using a compact CDPR prototype named DemoBot, and the results were compared to the predictions made by SEECR. Impressively, SEECR consistently provided accurate estimations of robot's behavior, regardless of the selected cable material and configuration.

While SEECR proves to be a valuable tool, it does have some limitations. It requires an initial guess of the MP pose deviation. Setting the guess to an estimated shift in the downward direction yielded accurate results. Furthermore, it is worth noting that SEECR may encounter difficulties when dealing with very high cable stiffness coefficients, but these are above the stiffness of cables currently used in CDPRs.

Future work includes adapting SEECR to fully-constrained CDPRs. Additionally, to enhance its capabilities, cable sag and mass will be taken into account. Finally, SEECR will be used to simulate the CDPR behavior with different control schemes.

REFERENCES

[1] J. Albus, R. Bostelman, and N. Dagalakis, "The nist spider, a robot crane," *Journal of research of the National Institute of Standards and Technology*, vol. 97, no. 3, pp. 373–385, 1992.

[2] A. Pott, C. Meyer, and A. Verl, "Large-scale assembly of solar power plants with parallel cable robots," in *ISR 2010 (41st International Symposium on Robotics) and ROBOTIK 2010 (6th German Conference on Robotics)*, pp. 1–6, VDE, 2010.

[3] S. Kawamura, H. Kino, and C. Won, "High-speed manipulation by using parallel wire-driven robots," *Robotica*, vol. 18, no. 1, pp. 13–21, 2000.

[4] G. Rosati, M. Andreolli, A. Biondi, and P. Gallina, "Performance of cable suspended robots for upper limb rehabilitation," in *2007 IEEE 10th International Conference on Rehabilitation Robotics*, pp. 385–392, IEEE, 2007.

[5] A. Pott, H. Mütherich, W. Kraus, V. Schmidt, P. Miermeister, and A. Verl, "Ipanema: a family of cable-driven parallel robots for industrial applications," in *Cable-Driven Parallel Robots (CableCon)*, pp. 119–134, Springer, 2013.

[6] M. Gouttefarde, J.-F. Collard, N. Riehl, and C. Baradat, "Geometry selection of a redundantly actuated cable-suspended parallel robot," *IEEE Transactions on Robotics*, vol. 31, no. 2, pp. 501–510, 2015.

[7] J.-P. Merlet, Y. Papegay, and A.-V. Gasc, "The prince's tears, a large cable-driven parallel robot for an artistic exhibition," in *2020 IEEE International Conference on Robotics and Automation (ICRA)*, pp. 10378–10383, IEEE, 2020.

[8] Z. Zaķe, N. Pedemonte, B. Moriniere, A. Suarez Roos, and S. Caro, "Elasto-static model and accuracy analysis of a large deployable cable-driven parallel robot," in *Cable-Driven Parallel Robots (CableCon)*, pp. 381–393, Springer, 2023.

[9] P. Miermeister, M. Lächele, R. Boss, C. Masone, C. Schenk, J. Tesch, M. Kerger, H. Teufel, A. Pott, and H. H. Bülthoff, "The cablerobot simulator large scale motion platform based on cable robot technology," in *2016 IEEE/RSJ International Conference on Intelligent Robots and Systems (IROS)*, pp. 3024–3029, IEEE, 2016.

[10] A. Pott, *Cable-Driven Parallel Robots: Theory and Application*. 2018.

[11] E. Picard, S. Caro, F. Plestan, and F. Claveau, "Stiffness oriented tension distribution algorithm for cable-driven parallel robots," in *Advances in Robot Kinematics 2020*, pp. 209–217, Springer, 2021.

[12] J. Bolboli, M. A. Khosravi, and F. Abdollahi, "Stiffness feasible workspace of cable-driven parallel robots with application to optimal design of a planar cable robot," *Robotics and Autonomous Systems*, vol. 114, pp. 19–28, 2019.

[13] S. Behzadipour and A. Khajepour, "Stiffness of cable-based parallel manipulators with application to stability analysis," *Journal of Mechanical Design*, vol. 128, no. 1, pp. 303–310, 2006.

[14] L. Gagliardini, *Discrete reconfigurations of cable-driven parallel robots*. PhD thesis, École Centrale de Nantes, 2016.

[15] W. Kraus, *Force control of cable-driven parallel robots*. PhD thesis, Universität Stuttgart, 2016.

[16] P. Miermeister, W. Kraus, T. Lan, and A. Pott, "An elastic cable model for cable-driven parallel robots including hysteresis effects," in *Cable-Driven Parallel Robots (CableCon)*, pp. 17–28, Springer, 2015.

[17] S. Baklouti, E. Courteille, S. Caro, and M. Dkhil, "Dynamic and oscillatory motions of cable-driven parallel robots based on a nonlinear cable tension model," *Journal of mechanisms and robotics*, vol. 9, no. 6, p. 061014, 2017.

[18] I. Chawla, P. M. Pathak, L. Notash, A. K. Samantaray, Q. Li, and U. K. Sharma, "Neural network-based inverse kineto-static analysis of cable-driven parallel robot considering cable mass and elasticity," in *Cable-Driven Parallel Robots (CableCon)*, pp. 50–62, Springer, 2021.

[19] U. A. Mishra and S. Caro, "Unsupervised neural network based forward kinematics for cable-driven parallel robots with elastic cables," in *Cable-Driven Parallel Robots (CableCon)*, pp. 63–76, Springer, 2021.

[20] H. Yuan, E. Courteille, and D. Deblaise, "Static and dynamic stiffness analyses of cable-driven parallel robots with non-negligible cable mass and elasticity," *Mechanism and Machine Theory*, vol. 85, pp. 64–81, 2015.

[21] M. H. Korayem, M. Bamdad, and M. Saadat, "Workspace analysis of cable-suspended robots with elastic cable," in *2007 IEEE International Conference on Robotics and Biomimetics (ROBIO)*, pp. 1942–1947, IEEE, 2007.

[22] J.-P. Merlet, "On the inverse kinematics of cable-driven parallel robots with up to 6 sagging cables," in *2015 IEEE/RSJ International Conference on Intelligent Robots and Systems (IROS)*, pp. 4356–4361, IEEE, 2015.

[23] E. Ottaviano and G. Castelli, "A study on the effects of cable mass and elasticity in cable-based parallel manipulators," in *ROMANSY 18 Robot Design, Dynamics and Control: Proceedings of The Eighteenth CISM-IFToMM Symposium*, pp. 149–156, Springer, 2010.

[24] D. Q. Nguyen, M. Gouttefarde, O. Company, and F. Pierrot, "On the simplifications of cable model in static analysis of large-dimension cable-driven parallel robots," in *2013 IEEE/RSJ International Conference on Intelligent Robots and Systems*, pp. 928–934, IEEE, 2013.

[25] M. Bamdad, F. Taheri, and N. Abtahi, "Dynamic analysis of a hybrid cable-suspended planar manipulator," in *2015 IEEE International Conference on Robotics and Automation (ICRA)*, pp. 1621–1626, IEEE, 2015.

[26] A. Phillips, A. Vinoo, and N. T. Fitter, "May i draw your attention? initial lessons from the large-scale generative mark maker," *IEEE Robotics and Automation Letters*, vol. 5, no. 2, pp. 691–698, 2020.

[27] P. Virtanen, R. Gommers, T. E. Oliphant, M. Haberland, T. Reddy, D. Cournapeau, E. Burovski, P. Peterson, W. Weckesser, J. Bright, S. J. van der Walt, M. Brett, J. Wilson, K. J. Millman, N. Mayorov, A. R. J. Nelson, E. Jones, R. Kern, E. Larson, C. J. Carey, İ. Polat, Y. Feng, E. W. Moore, J. VanderPlas, D. Laxalde, J. Perktold, R. Cimrman, I. Henriksen, E. A. Quintero, C. R. Harris, A. M. Archibald, A. H. Ribeiro, F. Pedregosa, P. van Mulbregt, and SciPy 1.0 Contributors, "SciPy 1.0: Fundamental Algorithms for Scientific Computing in Python," *Nature Methods*, vol. 17, pp. 261–272, 2020.

[28] G. Rubio-Gómez, D. Rodríguez-Rosa, J. A. García-Vanegas, A. Gonzalez-Rodríguez, F. J. Castillo-García, and E. Ottaviano, "Chain driven robots: An industrial application opportunity. a planar case approach," in *Cable-Driven Parallel Robots (CableCon)*, pp. 13–22, Springer, 2019.

[29] L. Barbazza, F. Oscari, S. Minto, and G. Rosati, "Trajectory planning of a suspended cable driven parallel robot with reconfigurable end effector," *Robotics and Computer-Integrated Manufacturing*, vol. 48, pp. 1–11, 2017.

[30] A. Pott, P. Tempel, A. Verl, and F. Wulle, "Design, implementation and long-term running experiences of the cable-driven parallel robot caro printer," in *Cable-Driven Parallel Robots (CableCon)*, pp. 379–390, Springer, 2019.

[31] A. L. C. Ruiz, S. Caro, P. Cardou, and F. Guay, "Arachnis: Analysis of robots actuated by cables with handy and neat interface software," in *Cable-Driven Parallel Robots: Proceedings of the Second International Conference on Cable-Driven Parallel Robots*, pp. 293–305, Springer, 2015.

[32] T. Rasheed, P. Long, and S. Caro, "Wrench-feasible workspace of mobile cable-driven parallel robots," *Journal of Mechanisms and Robotics*, vol. 12, no. 3, p. 031009, 2020.